Universality of jamming of nonspherical particles

Carolina Brito[a], Harukuni Ikeda (池田晴國)[b,1], Pierfrancesco Urbani[c], Matthieu Wyart[d], and Francesco Zamponi[b]

[a]Instituto de Física, Universidade Federal do Rio Grande do Sul, 91501-970 Porto Alegre, Brazil; [b]Laboratoire de Physique Theórique, Département de Physique de l'École Normale Supérieure, École Normale Supérieure, Paris Sciences et Lettres University, Sorbonne Université, CNRS, 75005 Paris, France; [c]Institut de Physique Théorique, Université Paris Saclay, CNRS, Commissariat à l'Énergie Atomique et aux Énergies Alternatives (CEA), F-91191 Gif-sur-Yvette, France; and [d]Institute of Physics, École Polytechnique Fédérale de Lausanne, CH-1015 Lausanne, Switzerland

Edited by Pablo G. Debenedetti, Princeton University, Princeton, NJ, and approved October 8, 2018 (received for review July 19, 2018)

Amorphous packings of nonspherical particles such as ellipsoids and spherocylinders are known to be hypostatic: The number of mechanical contacts between particles is smaller than the number of degrees of freedom, thus violating Maxwell's mechanical stability criterion. In this work, we propose a general theory of hypostatic amorphous packings and the associated jamming transition. First, we show that many systems fall into a same universality class. As an example, we explicitly map ellipsoids into a system of "breathing" particles. We show by using a marginal stability argument that in both cases jammed packings are hypostatic and that the critical exponents related to the contact number and the vibrational density of states are the same. Furthermore, we introduce a generalized perceptron model which can be solved analytically by the replica method. The analytical solution predicts critical exponents in the same hypostatic jamming universality class. Our analysis further reveals that the force and gap distributions of hypostatic jamming do not show power-law behavior, in marked contrast to the isostatic jamming of spherical particles. Finally, we confirm our theoretical predictions by numerical simulations.

jamming | glass | marginal stability | nonspherical particles

Upon compression, an athermal system consisting of purely repulsive particles suddenly acquires finite rigidity at a certain jamming transition density φ_J at which constituent particles start to touch each other, producing a finite mechanical pressure (1–3). The jamming transition is observed in a wide variety of physical, engineering, and biological systems such as metallic balls (4), foams (5, 6), colloids (7), polymers (8), candies (9), dices (10), and tissues (11). In the past decade, a lot of progress has been made in understanding the jamming transition of spherical and frictionless particles with repulsive interactions. Key findings involve (*i*) the power-law behaviors of the elastic modulus and contact number as a function of the proximity to φ_J (6, 12, 13), (*ii*) the emergence of excess soft modes in the vibrational density of states $D(\omega)$ (6), and (*iii*) the power-law divergence of the gap distribution function $g(h)$ and power-law tail of the force distribution function $P(f)$ at φ_J (6, 14–16). Those phenomena can be understood in terms of a marginal stability principle (17, 18): The system lies close to a mechanical instability. More precisely, at φ_J, the contact number per particle is $z_J = 2d$ (4, 6), which barely satisfies Maxwell's mechanical stability condition (19). Accepting marginal stability as a basic principle, one can successfully predict the critical exponents of soft spheres (17, 18) and derive a scaling relation between critical exponents of hard spheres (20–23). The importance of marginal stability is also highlighted by exact calculations for hard spheres in the large-dimension limit (15) and in a perceptron model of the jamming transition (24–26). These first-principle calculations prove that a full replica symmetric breaking (RSB) phase transition occurs ahead of the jamming transition. In the full RSB phase, the eigenvalue distribution function is gapless, and thus the system is indeed marginally stable (24). This approach provides exact results for the critical exponents, which agree well with the numerical results (15), once localized excitation modes are carefully separated (16, 22).

However, a system of spherical particles is an idealized model and, in reality, constituent particles are, in general, nonspherical. In this case, one should specify the direction of each particle in addition to the particle position. The effects of those extra degrees of freedom have been investigated in detail in the case of ellipsoids (2, 3, 9, 27–32). Notably, the contact number at the jamming point continuously increases from the isostatic value of spheres, as $z_J - 2d \propto \Delta^{1/2}$, where Δ denotes the deviation from the perfectly spherical shape. The system is thus hypostatic: The contact number is lower than what is expected by the naive Maxwell's stability condition, which would predict $z_J = 2(d + d_{\rm ex})$ where $d_{\rm ex}$ is the number of rotational degrees of freedom per particle (9, 28, 29). As a consequence of hypostaticity, $D(\omega)$ has anomalous zero modes at φ_J, which are referred to as "quartic modes" because they are stabilized by quartic terms of the potential energy (29–32). Hypostatic packings are also obtained for spherocylinders (33–37), superballs (38), superellipsoids (39), other convex-shaped particles (40), and even deformable polygons (41). Compared with spherical particles, the theoretical understanding of the jamming transition of nonspherical particles is still in its infancy (29, 42). In particular, the physical mechanism that induces a scaling behavior such as $z_J - 2d \propto \Delta^{1/2}$ is unclear.

In this work, we propose a theoretical framework to describe the universality class of hypostatic jamming. As a first example of universality, we map ellipsoids into a model of "breathing" spherical particles (BP), recently introduced in ref. 43. Based on the mapping, we show that the two models indeed have the same critical exponents by using a marginal stability argument. Next, we propose a generalization of the random perceptron model that mimics the BP and can be solved analytically using the replica method. We confirm that this model is in the same universality class of ellipsoids, BP, and other nonspherical particles that

Significance

The jamming transition is a key property of granular materials, including sand and dense suspensions. In the generic situation of nonspherical particles, its scaling properties are not completely understood. Previous empirical and theoretical work in ellipsoids and spherocylinders indicates that both structural and vibrational properties are fundamentally affected by shape. Here we explain these observations using a combination of marginal stability arguments and the replica method. We unravel a universality class for particles with internal degrees of freedom and derive how the structure of packings and their vibrations scale as the particles evolve toward spheres.

Author contributions: C.B., H.I., P.U., M.W., and F.Z. designed research, performed research, contributed new reagents/analytic tools, analyzed data, and wrote the paper.

The authors declare no conflict of interest.

This article is a PNAS Direct Submission.

[1]To whom correspondence should be addressed. Email: harukuni.ikeda@lpt.ens.fr.

display hypostatic jamming. This analysis further predicts the scaling behavior of $g(h)$ and $P(f)$ near the jamming point. Interestingly, we find that these functions do not show a power-law behavior even at the jamming point, in marked contrast to the jamming of spherical particles. Also the simplicity of the model allows us to derive an analytical expression of the density of states $D(\omega)$, which exhibits the very same scaling behavior as that of ellipsoids and BP. Finally, we confirm our predictions by numerical simulations of the BP model.

BP Model

The BP model (43) was originally introduced to understand the physics of the swap Monte Carlo algorithm (44), but here we focus on its relation with the jamming of ellipsoids. The model consists of N spherical particles with positions $\boldsymbol{x}_i$ in d dimensions and radius $R_i \geq 0$, interacting via the potential energy

$$V_N(\{\boldsymbol{x}\},\{R\}) = U_N(\{\boldsymbol{x}\},\{R\}) + \mu_N(\{R\}), \qquad [1]$$

where, defining $\theta(x)$ as the Heaviside theta function,

$$U_N = \sum_{i<j} k\frac{h_{ij}^2}{2}\theta(-h_{ij}), \quad h_{ij} = |\boldsymbol{x}_i - \boldsymbol{x}_j| - R_i - R_j, \qquad [2]$$

is the standard harmonic repulsive interaction potential of spherical particles such as bubbles and colloids (5), and the distribution of R_i, which can fluctuate around a reference value R_i^0, is controlled by the chemical potential term

$$\mu_N = \frac{k_R}{2}\sum_i (R_i - R_i^0)^2 \left(\frac{R_i^0}{R_i}\right)^2. \qquad [3]$$

Here, k_R is determined by imposing that the dimensionless SD $\Delta \propto \sqrt{\sum_i (R_i - R_i^0)^2/(NR_0^2)}$ is constant, with $R_0 = N^{-1}\sum_i R_i^0$. Note that $\Delta = 0$ (corresponding to $k_R = \infty$) gives back the usual spherical particles (5) and that the full distribution of radii, $P(R)$, can generically change even if Δ is kept fixed. Upon approaching jamming, where the adimensional pressure p (in units of kR_0^{2-d}) vanishes, it is found that $k_R = p/\Delta$ and $P(R)$ remains constant (43).

Because the BP model has Nd translational degrees of freedom and N radial degrees of freedom, the naive Maxwell stability condition requires $z \geq 2(d+1)$ in the thermodynamic limit (19, 45). However, a marginal stability argument and numerical simulations prove that the contact number at the jamming point z_J increases continuously as $z_J - 2d \propto \Delta^{1/2}$ (43) and the system is hypostatic for sufficiently small Δ; i.e., the number of constraints is smaller than that required by Maxwell's stability condition. This is very similar to ellipsoids and motivates us to conjecture that the two models could belong to the same universality class. In the following, we show that this expectation is indeed true: Hypostatic packings of the BP and ellipsoids are stabilized by a common mechanism and have the same critical exponents.

Mapping from Ellipsoids to BP

We now construct a mapping from a system of ellipsoids to the spherical BP model introduced above. Ellipsoids are described by their position $\boldsymbol{x}_i$ and by unit vectors $\hat{\boldsymbol{u}}_i$ along their principal axis, and for concreteness we model them by the Gay–Berne potential (31, 46)

$$V_N(\{\boldsymbol{x}\},\{\hat{\boldsymbol{u}}\}) = \sum_{i<j} v(h_{ij}), \quad v(h) = k\frac{h^2}{2}\theta(-h), \qquad [4]$$

where the gap function is defined as

$$h_{ij} = \frac{|\boldsymbol{x}_i - \boldsymbol{x}_j| - \sigma_{ij}}{\sigma_0},$$
$$\frac{\sigma_{ij}}{\sigma_0} = \frac{1}{\sqrt{1 - \frac{\chi}{2}\left(\frac{(\hat{\boldsymbol{r}}_{ij}\cdot\hat{\boldsymbol{u}}_i + \hat{\boldsymbol{r}}_{ij}\cdot\hat{\boldsymbol{u}}_j)^2}{1+\chi\hat{\boldsymbol{u}}_i\cdot\hat{\boldsymbol{u}}_j} + \frac{(\hat{\boldsymbol{r}}_{ij}\cdot\hat{\boldsymbol{u}}_i - \hat{\boldsymbol{r}}_{ij}\cdot\hat{\boldsymbol{u}}_j)^2}{1-\chi\hat{\boldsymbol{u}}_i\cdot\hat{\boldsymbol{u}}_j}\right)}}. \qquad [5]$$

Here, $\hat{\boldsymbol{r}}_{ij} = (\boldsymbol{x}_i - \boldsymbol{x}_j)/|\boldsymbol{x}_i - \boldsymbol{x}_j|$ is the unit vector connecting the ith and jth particles, $\varepsilon\sigma_0$ is the length of the principal axis, and $\chi = (\varepsilon^2 - 1)/(\varepsilon^2 + 1)$, where ε denotes the aspect ratio. Because we are interested in the nearly spherical case, we expand the pair potential in small $\Delta = \varepsilon - 1$ as

$$v(h_{ij}) = v(h_{ij}^{(0)}) - \frac{\Delta}{2}v'(h_{ij}^{(0)})\left[(\hat{\boldsymbol{r}}_{ij}\cdot\hat{\boldsymbol{u}}_i)^2 + (\hat{\boldsymbol{r}}_{ij}\cdot\hat{\boldsymbol{u}}_j)^2\right] + \Delta^2 w_{ij}, \qquad [6]$$

where $h_{ij}^{(0)} = r_{ij}/\sigma_0 - 1$ and $\Delta^2 w_{ij}$ denotes the $O(\Delta^2)$ term that we do not need to write explicitly. Substituting this in Eq. **4** and keeping terms up to Δ^2, we obtain $V_N \approx U_N + \mu_N$, where

$$U_N = \sum_{i<j}\left[v(h_{ij}^{(0)}) + \Delta^2 w_{ij}\right],$$
$$\mu_N = \frac{1}{2}\sum_i (\Delta\hat{\boldsymbol{u}}_i)\cdot k_i \cdot (\Delta\hat{\boldsymbol{u}}_i). \qquad [7]$$

The stiffness matrix is $k_i^{ab} = -\Delta^{-1}\sum_{j(\neq i)} v'(h_{ij}^{(0)})\hat{\boldsymbol{r}}_{ij}^a\hat{\boldsymbol{r}}_{ij}^b$, where $a, b = 1, \ldots, d$. Note that near the jamming point, k_i behaves as $k_i \sim v'(h)/\Delta \sim p/\Delta$, which is the same scaling of the stiffness k_R of the BP model, Eq. **3**. Hence, if we identify $\Delta\hat{\boldsymbol{u}}_i$ with R_i, in the vicinity of jamming the potential for ellipsoids can be analyzed essentially in the same way as in the BP model (43), as we discuss next.

Marginal Stability

The distinctive feature of both BP and ellipsoids is that the total potential, and thus the Hessian matrix, can be split into two parts: one having finite stiffness and the second one having vanishing stiffness p/Δ by dimensional arguments. The zero modes of the first term are stabilized by the second one, as recognized in refs. 29 and 32. We now provide additional insight on this structure by generalizing a marginal stability argument discussed for the BP in ref. 43. At jamming, $p = 0$ and $V_N = U_N$ because $\mu_N \propto p$. The $\mathcal{N}_3 \equiv Nz/2$ constraints coming from U_N, one per mechanical contact, stabilize the same number of vibrational modes. Because the system is hypostatic, there remain $\mathcal{N}_0 \equiv N(d + d_{\rm ex}) - Nz/2 = N(d_{\rm ex} - \delta z/2)$ zero-frequency modes, where $\delta z = z - 2d$ and $d_{\rm ex}$ is the number of extra degrees of freedom per particle; i.e., $d_{\rm ex} = 1$ for the BP and $d_{\rm ex} = d - 1$ for ellipsoids. Above jamming, where $p > 0$, the $\mathcal{N}_0$ zero modes are stabilized by the "soft" constraint coming from μ_N whose characteristic stiffness is $k_R \sim k_i \sim k(p/\Delta) \ll k$, where k is the stiffness associated to U_N. Hence, the energy scale of these modes remains well separated from that of the $\mathcal{N}_3$ other modes, and we can restrict to the $\mathcal{N}_0$-dimensional subspace of the soft modes. In this space, we have $\mathcal{N}_0 = N(d_{\rm ex} - \delta z/2)$ degrees of freedom, and μ_N provides $Nd_{\rm ex}$ constraints; hence the number of degrees of freedom is $N\delta z/2$ less than the number of constraints. When $\delta z \ll 1$, a variational argument developed in refs. 17 and 47 describes the low-frequency spectrum. It shows that the soft modes are shifted above a characteristic frequency $\omega_*^2 \sim k_i\delta z^2 \sim k_R\delta z^2 \sim \Delta^{-1}p\,\delta z^2$, which is reduced by $\sim -p$ by the so-called prestress terms, resulting in $\omega_*(p)^2 = c_1\Delta^{-1}p\delta z^2 - c_2 p$, where c_1 and c_2 are unknown constants. Assuming that the system is marginally stable, $\omega_*(p)=0$, results in (43)

$$\delta z \sim \Delta^{1/2}. \quad \textbf{[8]}$$

This explains the universal square-root singularity of the contact number z_J observed in ellipsoids, BP, and several other models (9, 29, 43), as illustrated in Fig. 1. Eq. **8** holds when $p \ll \Delta$, because in the argument we assumed to be close to jamming ($p \sim 0$) at fixed Δ. On the contrary, when $\Delta \ll p$, the contact number should have the same scaling of spherical particles:

$$\delta z \sim p^{1/2}. \quad \textbf{[9]}$$

Eqs. **8** and **9** imply that p and Δ have the same scaling dimension and the following scaling holds:

$$\delta z = \Delta^{\gamma} f\,(p/\Delta). \quad \textbf{[10]}$$

In the $\Delta \to 0$ limit, Eq. **10** reduces to Eq. **9**, which requires $\gamma = 1/2$ and $f(x) \to x^{1/2}$ for $x \gg 1$. In the $p \to 0$ limit, we should recover Eq. **8**, which requires $f(x) \to const$ for $x \ll 1$. For the BP, Eq. **10** is confirmed by numerical simulations (43). Assuming that $f(x)$ is a regular function around $x \sim 0$, one can expand it as $f(x) = c_0 + c_1 x + \cdots$ and obtains

$$z - z_J \sim \Delta^{-1/2} p, \quad \textbf{[11]}$$

where $z_J = 2d + c_0 \Delta^{1/2}$. This is compatible with previous numerical results of ellipsoids, where $z - z_J \sim \Delta^{-0.35 \pm 0.1} p$ (48). We can also study the response to shear deformation, which mainly excites the zero modes (30). Applying the argument in ref. 18 to the zero modes and using Eq. **8**, the shear modulus G behaves as $G \sim \delta z k_R \sim \delta z k_i \sim p/\sqrt{\Delta}$, in perfect agreement with the numerical result (30).

Vibrational Spectrum

The marginal stability argument suggests that $\mathcal{N}_0$ soft vibrational modes can be found in the frequency range $\omega^* \lesssim \omega \lesssim \sqrt{k_R}$, with $\omega^* \sim 0$ due to marginal stability and $k_R \sim p/\Delta$, while the remaining $\mathcal{N}_3$ modes have finite frequency at jamming. We now refine the argument to discuss in more detail the vibrational density of states $D(\omega)$. It is convenient to define the $\mathcal{N} \times \mathcal{N}$ Hessian matrix of the BP model, with $\mathcal{N} = N(d + d_{\rm ex})$, as the second derivative of the interaction potential V_N w.r.t. $\boldsymbol{x}_i$ and R_i/Δ, in such a way that it has a similar scaling to the one of ellipsoids, where R_i/Δ is mapped onto the angular degrees of freedom $\hat{\boldsymbol{u}}$.

Then, $D(\omega)$ near jamming can be separated into the following three regions: (*i*) The lowest band corresponds to the $\mathcal{N}_0 = N(d_{\rm ex} - \delta z/2)$ zero modes stabilized by μ_N. Their typical frequency is $\omega_0^2 \sim \partial^2 \mu_N / \partial(\Delta^{-1} R_i)^2 \sim k_R \Delta^2 \sim \Delta p$. The remaining $\mathcal{N}_3 = \mathcal{N} - \mathcal{N}_0 = Nz/2$ modes can be split into two bands: (*ii*) an intermediate band corresponding to the extra (rotational or radial) degrees of freedom $\mathcal{N}_1 = N\delta z/2$, with typical frequency $\omega_1^2 \sim \partial^2 V_N / \partial(\Delta^{-1} R_i)^2 \sim \Delta^2$, and (*iii*) the highest band corresponding to the $\mathcal{N}_2 = Nd$ translational degrees of freedom. For $\Delta \ll 1$, the additional degrees of freedom do not strongly affect these modes, and one can apply the standard variational argument of spherical particles (17, 47), which predicts that their typical frequency is $\omega_2^2 \sim \delta z^2 \sim \Delta$. The resulting $D(\omega)$ differs significantly from that of isostatic packings of spherical particles, which displays a single translational band.

Numerical results for $D(\omega)$ of ellipsoids from ref. 30 and of the BP from ref. 43 and analytical results for the perceptron model introduced below are reported in Fig. 2. Details about the simulations of the BP are explained in ref. 43; here we show data for $N = 484$ particles, averaged over at least 1,000 samples for each state point. As predicted by our theory, $D(\omega)$ consists of three separated bands with characteristic peak frequencies $\omega_{0,1,2}$. Their scaling with Δ, also reported in Fig. 2 at fixed p, follows the theoretical predictions $\omega_0 \propto \Delta^{1/2}$, $\omega_1 \propto \Delta$, and $\omega_2 \propto \Delta^{1/2}$. We also find that $\omega_0 \propto p^{1/2}$ for small p, while $\omega_{1,2}$ do not change much with p, which is again consistent with the theory. Finally, in Fig. 3 we report the fraction $f_i = \mathcal{N}_i/\mathcal{N}$ of modes in each band for the BP, which also follow the theoretical prediction as a function of Δ and p.

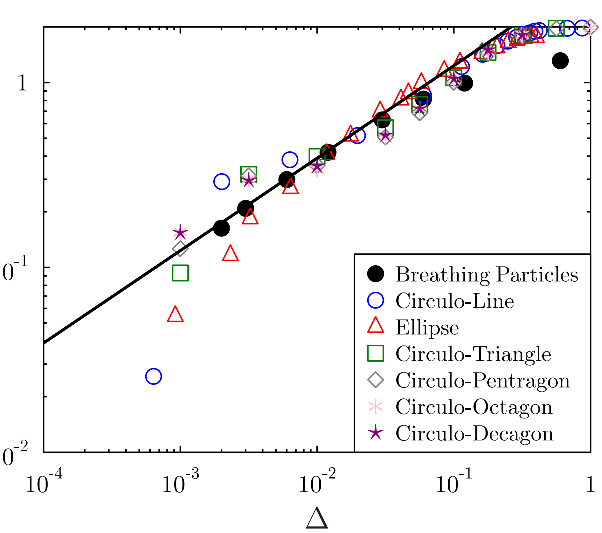

Fig. 1. Universal scaling of the contact number. Symbols denote the numerical result, while the solid line denotes the theoretical prediction $\delta z \sim \Delta^{1/2}$. Data for nonspherical particles are reproduced from ref. 40, and from the sphericity A, we defined $\Delta = c(A-1)^{1/2}$, which recovers the correct scaling relation between the sphericity and aspect ratio of ellipses for small Δ. We set $c = 1/6$ to collapse all data. Data for the BP correspond to a pressure $p = 10^{-6}$.

Mean-Field Model

The universality class of isostatic jamming is well understood: It can be described analytically by particles in $d \to \infty$ (15) or, equivalently, by the perceptron model (24–26). Both models reproduce the critical exponents of isostatic jamming in all dimensions d, leading to the conjecture that its lower critical dimension is $d = 2$ (49).

We now introduce a mean-field model which describes the universality class of hypostatic jamming in the BP, ellipsoids, and many other models of nonspherical particles. The model, which is a generalization of the perceptron, can be solved analytically and, as we show, the solution reproduces all of the critical exponents of hypostatic jamming. It consists of one tracer particle with coordinate $\boldsymbol{x}$ on the surface of the N-dimensional hypersphere of radius $\sqrt{N}$ and M obstacles of coordinates $\boldsymbol{\xi}_\mu$ and "size" $\sigma + R_\mu$. The interaction potential between the tracer particle and the obstacles is

$$V_N = U_N + \mu_N, \;\; U_N = \sum_{\mu=1}^{M} v(h_\mu), \;\; \mu_N = \frac{k_R}{2} \sum_{\mu=1}^{M} R_\mu^2, \quad \textbf{[12]}$$

where $v(h) = h^2 \theta(-h)/2$ and the gap variable h_μ is defined as

$$h_\mu = \frac{\boldsymbol{x} \cdot \boldsymbol{\xi}_\mu}{\sqrt{N}} - \sigma - R_\mu. \quad \textbf{[13]}$$

The $\boldsymbol{\xi}_\mu$ are frozen variables, and each of their components follows independently a normal distribution of zero mean and unit

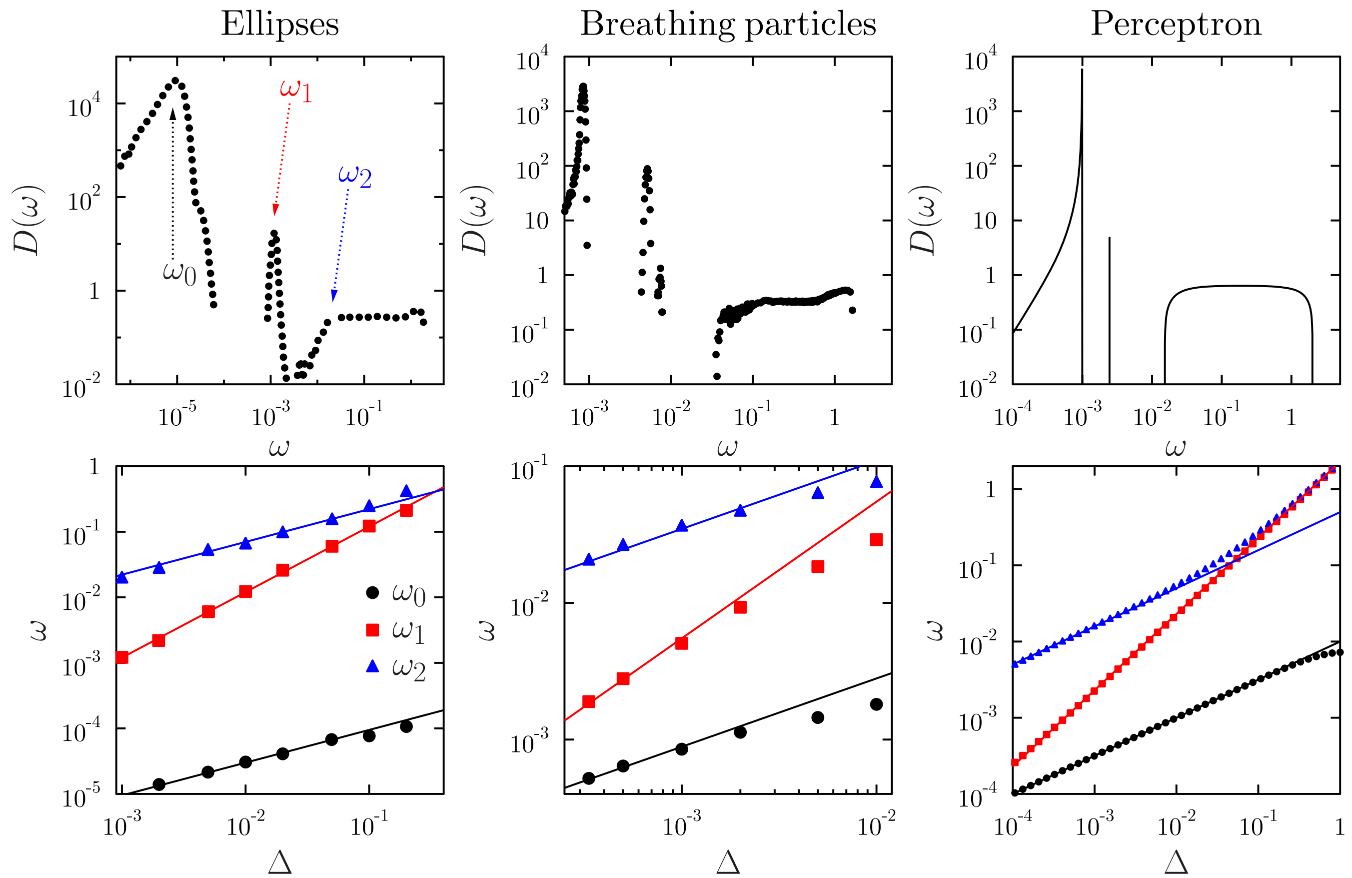

Fig. 2. Universality of the density of states. (*Top*) Density of states for ellipses, BP, and the perceptron. (*Bottom*) Evolution with Δ of the characteristic frequencies at $p = 10^{-4}$. Solid lines denote the theoretical predictions, $\omega_0 \propto \Delta^{1/2}$, $\omega_1 \propto \Delta$, and $\omega_2 \propto \Delta^{1/2}$, respectively. Data of ellipses are reproduced from ref. 32.

variance. The dynamical variables are $\boldsymbol{x}$ and the R_μ, whose variance is controlled by the chemical potential μ_N. We fix the value of k_R so that $\sum_{\mu=1}^{M} R_\mu^2 = M\Delta^2$. In the $\Delta \to 0$ limit, the system reduces to the standard perceptron model investigated in ref. 26, while for $\Delta > 0$ the R_μ play the same role as the particle sizes in the BP model.

Because the model can be solved by the same procedure as that of the standard perceptron model, here we give just a brief sketch of our calculation. The free energy of the model at temperature $T = 1/\beta$ can be calculated by the replica method, $-\beta f = \lim_{n\to 0} \frac{1}{nN} \log \overline{Z^n}$, where $Z = \int d^N\boldsymbol{x} d^M R e^{-\beta V_N}$ and the overbar denotes the averaging over the quenched randomness $\boldsymbol{\xi}_\mu$. Here we are interested in the athermal limit $T \to 0$. Using the saddle-point method, the free energy can be expressed as a function of the overlap $q_{ab} = \langle \boldsymbol{x}^a \cdot \boldsymbol{x}^b \rangle / N$, where $\boldsymbol{x}^a$ and $\boldsymbol{x}^b$ denote the positions of the tracer particles of the ath and bth replicas, respectively. In the $n \to 0$ limit, q_{ab} is parameterized by a continuous variable $x \in [0,1]$, $q_{ab} \to q(x)$. The function $q(x)$ plays the role of the order parameter and characterizes the hierarchical structure of the metastable states (50). We first calculate the phase diagram assuming a constant $q(x) = q$, which is the so-called replica symmetric (RS) ansatz that describes an energy landscape with a single minimum. The result for $\Delta = 0.1$ is shown in Fig. 4. The control parameters are the obstacle density $\alpha = M/N$ and size σ. If α is small, the tracer particle can easily find islands of configurations $\boldsymbol{x}$ that satisfy all of the constraints $h_\mu > 0$: The total potential energy U_N and the pressure vanish and the system is unjammed. The overlap $q < 1$ measures the typical distance between two zero-energy configurations. Upon increasing α, q increases and eventually reaches $q = 1$ at α_J, which is the jamming transition point (Fig. 4). Naturally, due to the additional degrees of freedom when $\Delta > 0$, we have $\alpha_J(\Delta) > \alpha_J(0)$ for equal σ. For $\sigma > 0$, the RS ansatz is stable for all values of α and it describes the jamming transition. For $\sigma < 0$ instead, the jamming line is surrounded by a RSB region where the RS ansatz is unstable. The jamming transition should thus be described by the RSB ansatz where $q(x)$ is not constant, corresponding to a rough energy landscape. The qualitative behavior of the phase diagram is independent of Δ; in

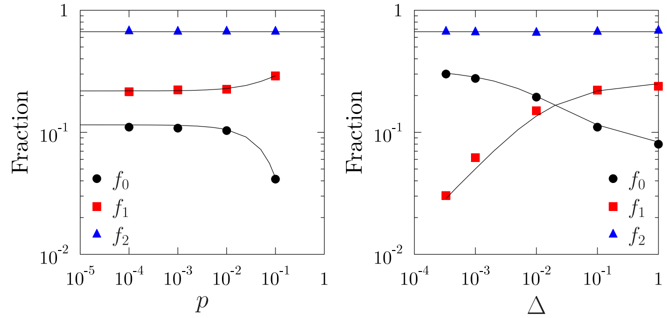

Fig. 3. Weights of the density of states. Shown is the fraction of modes $f_i = \mathcal{N}_i/\mathcal{N}$ in the three bands of $D(\omega)$ given in Fig. 2, plotted as functions of p at fixed $\Delta = 10^{-1}$ (*Left*) and Δ at fixed $p = 10^{-4}$ (*Right*) for BP (with $d = 2$ and $d_{\rm ex} = 1$). The theoretical predictions $f_0 = (1 - \delta z/2)/3$, $f_1 = \delta z/6$, and $f_2 = 2/3$ are plotted as solid lines, inferred from the measured δz.

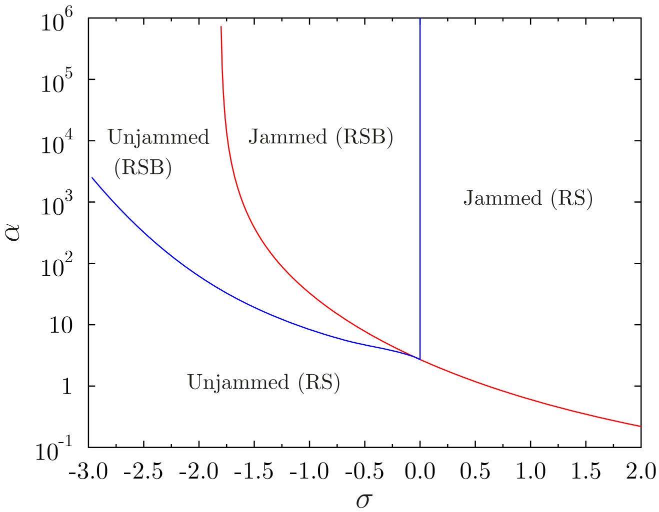

Fig. 4. The phase diagram of the perceptron model for $\Delta = 0.1$. The red line denotes the jamming point. The blue lines denote the RSB instability. The jamming line in the nonconvex region ($\sigma < 0$) is surrounded by the RSB lines.

particular, the jamming line for $\sigma < 0$ is always surrounded by a RSB region.

An important observable to characterize jamming is the gap distribution $\rho(h) \equiv \frac{1}{N}\sum_{\mu=1}^{M}\langle\delta(h_\mu - h)\rangle$ that also gives the contact number $z = \int_{-\infty}^{0} dh\rho(h)$. At jamming, z counts the gaps h_μ that are exactly equal to zero. For comparison with numerical results, we introduce the positive gap distribution $g(h) \equiv \theta(h)\rho(h)/\int_0^\infty dh\rho(h)$ and the force distribution $P(f) \equiv \theta(-h)\rho(h)\frac{\partial h}{\partial f}/\int_{-\infty}^{0}\rho(h)\frac{\partial h}{\partial f}df$, where $f = -h/p$ (corresponding to negative gaps), both normalized to 1. For the standard perceptron model with $\Delta = 0$ and $\sigma < 0$, jamming is isostatic with $z = 1$ (26), and both $g(h)$ and $P(f)$ exhibit a power-law behavior (24–26). In the jammed phase and $\alpha \gtrsim \alpha_J$, the system is described by a "regular" full RSB solution where $1 - q(x) \sim y_\chi^2 x^{-2}$ for $q(x) \sim 1$, and $g(h)$ and $P(f)$ are regular and finite functions. The prefactor y_χ is predominantly controlled by the contact number z and diverges at isostaticity when $z = 1$ (26) and the regular solution breaks down. At α_J, the model is described by the "jamming" solution where $1 - q(x) \sim x^{-\kappa}$, $g(h) \sim h^{-\gamma}$, and $P(f) \sim f^\theta$, with critical exponents $\kappa \simeq 1.42$, $\gamma = (2-\kappa)/\kappa$, and $\theta = (3\kappa - 4)/(2-\kappa)$ (15, 24–26). Near α_J, the regular solution should connect to the jamming solution. This matching argument leads to $z - 1 \sim p^{1/2}$, which is the same scaling behavior as that of spherical particles (6).

The situation is completely different if $\Delta > 0$. One can show that the contact number at jamming is $z_J \geq 1$, meaning that the regular solution persists even at α_J. Consequently, $g(h)$ and $P(f)$ are finite and regular functions at jamming, and the square-root behavior of the contact number is replaced by $z - z_J = c_\Delta p$. At α_J, the regular solution should connect to the jamming solution in the limit of $\Delta \to 0$. Using the form of the scaling solution derived for $\Delta \to 0$ in ref. 26 and $z - z_J \sim p$, this matching argument leads to the scaling behavior of $g(h)$ and $P(f)$ at α_J:

$$g(h) \sim \begin{cases} \Delta^{-\mu\gamma} p_0(h\Delta^{-\mu}) & (h \sim \Delta^\mu) \\ h^{-\gamma} & (h \sim 1) \end{cases}, \qquad [14]$$

$$P(f) \sim \begin{cases} \Delta^{\theta\nu} p_0(f\Delta^{-\nu}) & (f \sim \Delta^\nu) \\ f^\theta & (f \sim 1) \end{cases}, \qquad [15]$$

with new critical exponents $\mu = \kappa/(4\kappa - 4) = 0.851$ and $\nu = \mu - 1/2$ and a universal scaling function $p_0(x)$. The scaling analysis also leads to $z_J - 1 \sim \Delta^{1/2}$ and $c_\Delta \sim \Delta^{-1/2}$, consistent with the marginal stability argument, Eqs. **8** and **11**.

The simplicity of the model allows us to derive the analytical form of the density of states $D(\omega)$. As before, we define the Hessian matrix as the second derivatives of the interaction potential V_N, Eq. **12**, w.r.t. x_i and R_μ/Δ. Using the Edwards–Jones formula for the eigenvalue density $\rho(\lambda)$ (51, 52), the density of states $D(\omega) = 2\omega\rho(\omega^2)$ can be expressed analytically in closed form as a function of z, k_R, and p. These quantities should be obtained by solving numerically the full RSB equations but for simplicity, because here we are interested only in the scaling properties of $D(\omega)$, to obtain Fig. 2 we used arbitrary functions z, k_R, and p which are compatible with the analytical scaling derived from the full RSB equation. We find that $D(\omega)$ displays three separate bands (Fig. 2). As in the standard perceptron (24), marginal stability in the full RSB phase implies that the lowest band starts from $\omega = 0$ and for small ω, $D(\omega) \sim \omega^2$. The lowest band terminates at $\omega_0 \sim \Delta^{1/2}p^{1/2}$ near which $D(\omega)$ exhibits a sharp peak. At $\omega_1 \sim \Delta$ a delta peak is found, while the highest band starts from $\omega_2 \sim \Delta^{1/2}$. The qualitative behavior of $D(\omega)$ and the scaling of ω_0, ω_1, and ω_2 are the same as those of all of the models displaying hypostatic jamming, such as ellipsoids (31, 32) and BP (43). This confirms that the generalized perceptron can reproduce analytically all of the critical properties of the hypostatic jamming transition.

As a final check of universality, we test the prediction for the Δ dependence of the gap distribution function $g(h)$ at the jamming point, Eq. **14**. In Fig. 5, we show numerical results (obtained as in ref. 43) for $g(h)$ of the BP model at $p = 10^{-5}$, a value small enough to observe the critical behavior. Here, as usual for particle systems, $g(h)$ is normalized by $g(h) \to 1$ for larger h. When $\Delta = 0$, $g(h)$ exhibits a power-law divergence, $g(h) \sim h^{-\gamma}$, where $\gamma = 0.413$, consistent with previous numerical observation (6, 14, 15). For finite Δ, on the contrary, the divergence of $g(h)$ is cut off (Fig. 5), consistent with the theoretical prediction of Eq. **14**.

Conclusions

Using a marginal stability argument, we derived the scaling behavior of the contact number z and the density of states $D(\omega)$ of ellipsoids and breathing particles. Our theory predicts that the scaling behaviors of the two models are identical, which we confirmed numerically. Many other models of nonspherical particles display the same jamming criticality (40), which defines another universality class of hypostatic jamming. We

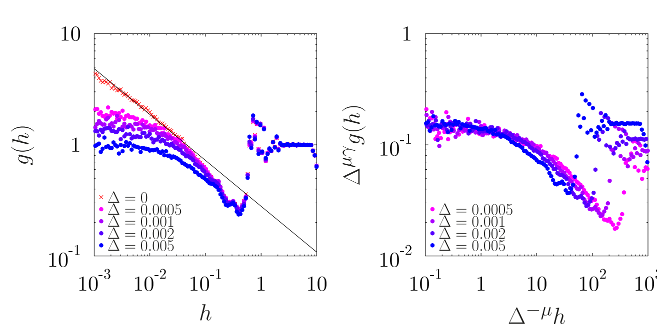

Fig. 5. Gap distribution $g(h)$ of BP near the jamming point, $p = 10^{-6}$. (*Left*) Symbols denote the numerical result, while the solid line denotes the theoretical prediction, $g(h) \propto h^{-0.413}$. (*Right*) Scaling plot of the same data according to Eq. **14**.

introduced an analytically solvable model which allows us to derive analytically the critical exponents associated to this universality class.

One of the most surprising outputs of our theory is the universality of the density of states $D(\omega)$ (Fig. 2). This might be relevant for some colloidal experiments where the constituents are nonspherical (53), in which the vibrational modes could be experimentally extracted from the fluctuations of positions (54, 55). Another relevant question is how nonspherical particles would flow under shear (30). The divergence of the viscosity at jamming is related to the low eigenvalues of $D(\omega)$ (56), which suggests that the shear flow of nonspherical particles should be quite different from that of spherical particles, in agreement with recent experiments (57).

ACKNOWLEDGMENTS. We thank B. Chakraborty, A. Ikeda, J. Kurchan, S. Nagel, and S. Franz for interesting discussions. We thank the authors of refs. 40 and 32 for sharing their data used in Figs. 1 and 2, respectively. This project received funding from the European Research Council under the European Union's Horizon 2020 Research and Innovation program (Grant 723955-GlassUniversality). This work was supported by Grants 689 454953 (to M.W.) and 454955 (to F.Z.) from the Simons Foundation and by a public grant from the "Laboratoire d'Excellence Physics Atoms Light Mater" (LabEx PALM) overseen by the French National Research Agency (ANR) as part of the "Investissements d'Avenir" program (reference no. ANR-10-LABX-0039-PALM; to P.U.).

1. Liu AJ, Nagel SR, van Saarloos W, Wyart M (2010) *The Jamming Scenario: An Introduction and Outlook*, eds Berthier L, Biroli G, Bouchaud J, Cipeletti L, van Saarloos W (Oxford Univ Press, Oxford).
2. Van Hecke M (2009) Jamming of soft particles: Geometry, mechanics, scaling and isostaticity. *J Phys Condens Matter* 22:033101.
3. Torquato S, Stillinger FH (2010) Jammed hard-particle packings: From Kepler to Bernal and beyond. *Rev Mod Phys* 82:2633–2672.
4. Bernal J, Mason J (1960) Packing of spheres: Co-ordination of randomly packed spheres. *Nature* 188:910–911.
5. Durian DJ (1995) Foam mechanics at the bubble scale. *Phys Rev Lett* 75:4780–4783.
6. O'Hern CS, Silbert LE, Liu AJ, Nagel SR (2003) Jamming at zero temperature and zero applied stress: The epitome of disorder. *Phys Rev E* 68:011306.
7. Zhang Z, et al. (2009) Thermal vestige of the zero-temperature jamming transition. *Nature* 459:230–233.
8. Karayiannis NC, Foteinopoulou K, Laso M (2009) The structure of random packings of freely jointed chains of tangent hard spheres. *J Chem Phys* 130:164908.
9. Donev A, et al. (2004) Improving the density of jammed disordered packings using ellipsoids. *Science* 303:990–993.
10. Jaoshvili A, Esakia A, Porrati M, Chaikin PM (2010) Experiments on the random packing of tetrahedral dice. *Phys Rev Lett* 104:185501.
11. Bi D, Lopez J, Schwarz J, Manning ML (2015) A density-independent rigidity transition in biological tissues. *Nat Phys* 11:1074–1079.
12. O'Hern CS, Langer SA, Liu AJ, Nagel SR (2002) Random packings of frictionless particles. *Phys Rev Lett* 88:075507.
13. Ellenbroek WG, Somfai E, van Hecke M, van Saarloos W (2006) Critical scaling in linear response of frictionless granular packings near jamming. *Phys Rev Lett* 97: 258001.
14. Donev A, Torquato S, Stillinger FH (2005) Pair correlation function characteristics of nearly jammed disordered and ordered hard-sphere packings. *Phys Rev E* 71: 011105.
15. Charbonneau P, Kurchan J, Parisi G, Urbani P, Zamponi F (2014) Fractal free energy landscapes in structural glasses. *Nat Commun* 5:3725.
16. Charbonneau P, Corwin EI, Parisi G, Zamponi F (2015) Jamming criticality revealed by removing localized buckling excitations. *Phys Rev Lett* 114:125504.
17. Wyart M, Silbert LE, Nagel SR, Witten TA (2005) Effects of compression on the vibrational modes of marginally jammed solids. *Phys Rev E* 72:051306.
18. Wyart M (2006) On the rigidity of amorphous solids. *Ann Phys Fr* 30:3.
19. Maxwell JC (1864) L. on the calculation of the equilibrium and stiffness of frames. *Lond Edinb Dublin Philos Mag J Sci* 27:294–299.
20. Brito C, Wyart M (2006) On the rigidity of a hard-sphere glass near random close packing. *Europhys Lett* 76:149–155.
21. Wyart M (2012) Marginal stability constrain force and pair distributions at random close packing. *Phys Rev Lett* 109:125502.
22. Lerner E, Düring G, Wyart M (2013) Low-energy non-linear excitations in sphere packings. *Soft Matter* 9:8252–8263.
23. DeGiuli E, Lerner E, Brito C, Wyart M (2014) Force distribution affects vibrational properties in hard-sphere glasses. *Proc Natl Acad Sci USA* 111:17054–17059.
24. Franz S, Parisi G, Urbani P, Zamponi F (2015) Universal spectrum of normal modes in low-temperature glasses. *Proc Natl Acad Sci USA* 112:14539–14544.
25. Franz S, Parisi G (2016) The simplest model of jamming. *J Phys A Math Theor* 49:145001.
26. Franz S, Parisi G, Sevelev M, Urbani P, Zamponi F (2017) Universality of the SAT-UNSAT (jamming) threshold in non-convex continuous constraint satisfaction problems. *SciPost Phys* 2:019.
27. Man W, et al. (2005) Experiments on random packings of ellipsoids. *Phys Rev Lett* 94:198001.
28. Delaney G, Weaire D, Hutzler S, Murphy S (2005) Random packing of elliptical disks. *Philos Mag Lett* 85:89–96.
29. Donev A, Connelly R, Stillinger FH, Torquato S (2007) Underconstrained jammed packings of nonspherical hard particles: Ellipses and ellipsoids. *Phys Rev E* 75:051304.
30. Mailman M, Schreck CF, O'Hern CS, Chakraborty B (2009) Jamming in systems composed of frictionless ellipse-shaped particles. *Phys Rev Lett* 102:255501.
31. Zeravcic Z, Xu N, Liu A, Nagel S, van Saarloos W (2009) Excitations of ellipsoid packings near jamming. *Europhys Lett* 87:26001.
32. Schreck CF, Mailman M, Chakraborty B, O'Hern CS (2012) Constraints and vibrations in static packings of ellipsoidal particles. *Phys Rev E* 85:061305.
33. Williams SR, Philipse AP (2003) Random packings of spheres and spherocylinders simulated by mechanical contraction. *Phys Rev E* 67:051301.
34. Blouwolff J, Fraden S (2006) The coordination number of granular cylinders. *Europhys Lett* 76:1095–1101.
35. Wouterse A, Williams SR, Philipse AP (2007) Effect of particle shape on the density and microstructure of random packings. *J Phys Condens Matter* 19:406215.
36. Wouterse A, Luding S, Philipse A (2009) On contact numbers in random rod packings. *Granular Matter* 11:169–177.
37. Marschall T, Teitel S (2018) Compression-driven jamming of athermal frictionless spherocylinders in two dimensions. *Phys Rev E* 97:012905.
38. Jiao Y, Stillinger FH, Torquato S (2010) Distinctive features arising in maximally random jammed packings of superballs. *Phys Rev E* 81:041304.
39. Delaney GW, Cleary PW (2010) The packing properties of superellipsoids. *Europhys Lett* 89:34002.
40. VanderWerf K, Jin W, Shattuck MD, O'Hern CS (2018) Hypostatic jammed packings of frictionless nonspherical particles. *Phys Rev E* 97:012909.
41. Boromand A, Signoriello A, Ye F, O'Hern CS, Shattuk M (2018) Jamming of deformable polygons. arXiv:1801.06150. Preprint, posted January 18, 2018.
42. Baule A, Mari R, Bo L, Portal L, Makse HA (2013) Mean-field theory of random close packings of axisymmetric particles. *Nat Commun* 4:2194.
43. Brito C, Lerner E, Wyart M (2018) Theory for swap acceleration near the glass and jamming transitions for continuously polydisperse particles. *Phys Rev X* 8:031050.
44. Ninarello A, Berthier L, Coslovich D (2017) Models and algorithms for the next generation of glass transition studies. *Phys Rev X* 7:021039.
45. Alexander S (1998) Amorphous solids: Their structure, lattice dynamics and elasticity. *Phys Rep* 296:65–236.
46. Gay J, Berne B (1981) Modification of the overlap potential to mimic a linear site–site potential. *J Chem Phys* 74:3316–3319.
47. Yan L, DeGiuli E, Wyart M (2016) On variational arguments for vibrational modes near jamming. *Europhys Lett* 114:26003.
48. Schreck CF, Xu N, O'Hern CS (2010) A comparison of jamming behavior in systems composed of dimer-and ellipse-shaped particles. *Soft Matter* 6:2960–2969.
49. Goodrich CP, Liu AJ, Nagel SR (2012) Finite-size scaling at the jamming transition. *Phys Rev Lett* 109:095704.
50. Mézard M, Parisi G, Virasoro M (1987) *Spin Glass Theory and Beyond: An Introduction to the Replica Method and Its Applications* (World Scientific, Singapore), Vol 9.
51. Edwards SF, Jones RC (1976) The eigenvalue spectrum of a large symmetric random matrix. *J Phys A Math Gen* 9:1595–1603.
52. Livan G, Novaes M, Vivo P (2018) *Introduction to Random Matrices: Theory and Practice*. SpringerBriefs in Mathematical Physics (Springer, Cham, Switzerland).
53. Kim JW, Larsen RJ, Weitz DA (2006) Synthesis of nonspherical colloidal particles with anisotropic properties. *J Am Chem Soc* 128:14374–14377.
54. Chen K, et al. (2010) Low-frequency vibrations of soft colloidal glasses. *Phys Rev Lett* 105:025501.
55. Ghosh A, Chikkadi VK, Schall P, Kurchan J, Bonn D (2010) Density of states of colloidal glasses. *Phys Rev Lett* 104:248305.
56. Lerner E, Düring G, Wyart M (2012) A unified framework for non-Brownian suspension flows and soft amorphous solids. *Proc Natl Acad Sci USA* 109:4798–4803.
57. Tapia F, Shaikh S, Butler JE, Pouliquen O, Guazzelli E (2017) Rheology of concentrated suspensions of non-colloidal rigid fibres. *J Fluid Mech* 827:718–740.